Underwater acoustic communications: Long term test of turbo equalization in shallow water

Roald Otnes, *Member, IEEE*, and Trym H. Eggen, *Member, IEEE*

Abstract

Acoustic telemetry sea trials lasting for three months with experiment periods of 7 hours have been carried out, using a turbo receiver. The communication channel is shallow; the depth is approximately 10 m and the range is 850 m, showing variable multipath. The wind speed and the sound speed profile (SSP) is measured during some of the experiments. The results show reliable communication over the entire period, and performance improvement of the turbo receiver compared to a decision feedback equalizer (DFE) used as reference receiver. The noise in the experiment data suggests significant deviations from the Gaussian assumption, and analysis of turbo receiver performance under heavy-tailed noise is presented.

I. Introduction

In this paper, we present results from an underwater acoustic communications trial extending over a period of 3 months. The modulation schemes used are 4- and 8-PSK (phase shift keying) with error–correction coding and BPSK (binary PSK) training sequences. The received signals are stored to file and processed off-line, using iterative channel estimation, equalization, and decoding (turbo equalization).

Since 1995, the concept of turbo equalization, or iterative equalization and decoding, has been extensively studied in the communications literature [1]–[4]. This principle for joint equalization

The author R. Otnes is with the Norwegian Defence Research Establishment (FFI), PO box 115, NO-3191 Horten, Norway, email: roald.otnes@ffi.no. The author T. H. Eggen was with Kongsberg Maritime, PO box 111, NO-3191 Horten, Norway, at the time of manuscript submission. He is now with GE Vingmed Ultrasound, email: trym.eggen@ge.com. The two authors have contributed equal amounts to the work described herein.

Dette er en postprint-versjon / This is a postprint version.
DOI til publisert versjon / DOI to published version: 10.1109/JOE.2008.925893

and decoding can be applied whenever the transmitter consists of an encoder for an error-correcting code (ECC) and an interleaver permuting the code bits before they are mapped onto a signal constellation and transmitted over an intersymbol interference (ISI) channel.

Initial works on turbo equalization, e.g., [1], [4], assume the channel impulse response (CIR) to be known. When the CIR is unknown and time-varying, as in underwater communication systems, channel estimation and tracking is required. When turbo equalization is used in the receiver, it is possible to improve the channel estimate over the iterations by including the channel tracking algorithm in the iterative loop (using soft symbols fed back from the decoder as "training symbols" between the ordinary training sequences). For further details on this topic see [5] and references therein.

There is a large body of literature reporting results from underwater telemetry experiments. Examples include [6] which considers DPSK (differential PSK) signalling over a channel which does not suffer from multipath, [7]–[10] which consider PSK signalling with different single- and multi-channel adaptive equalization techniques, [11] which considers different multiple-input/multiple-output (MIMO) techniques, [12] which uses time reversal array techniques, and [13], [14] which consider different turbo receiver techniques. For a complete literature review on underwater communication experiments up to 1999 we refer to [15]. A common feature of these reports is the focus on a single transmission or short term experiments.

The major contribution of this paper is results from long term testing. To our knowledge, variations in channel conditions for the same path over a period of several months have not previously been presented. The ocean environment is highly variable, with time scales varying from a few ms to several weeks. The series of experiments reported herein spans three months in shallow water. One issue is to look for correlation between environment parameters, such as sound speed profile and wind speed, and receiver performance in terms of error rates.

Another contribution of the paper is the analysis of turbo receiver performance with heavy-tailed noise, modelled as having a normal inverse Gaussian (NIG) distribution. This noise assumption is motivated by the extensive data available. It is also shown by simulations that receiver performance can be improved if the actual noise statistics are used in the demapper equations.

In Section II we briefly summarize the experiment setup before continuing with a discussion of the environmental parameters in Section III. The sea trials and the corresponding results are

shown in Section IV. We proceed with a presentation of the receiver in Section V and case studies on its performance in Section VI. The receiver performance under heavy-tailed noise statistics is studied in Section VII. We summarize the results in Section VIII.

II. Experimental setup

The locations of the transmit (TX) and receive (RX) subsystems are marked at the map in Fig. 1. This figure shows water depths ranging from 5 to 15 m. The range between RX and TX

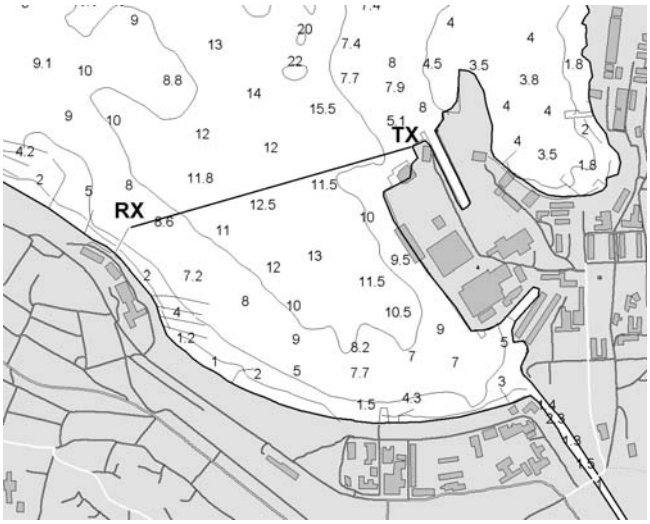

Fig. 1. Map of the area for the communication experiments in the inner harbor of Horten, Norway. Depths are in m.

is 850 m, thus the communication channel is very shallow. The shipping activity in this area is moderate, consisting of a small number of larger vessels (e.g., ferries), and a larger number of speed boats, yachts, etc.

A. Transmit side

The transmitter is mounted at the end of a pier. It is fixed, with a metal rod clamped to the concrete of the pier. The transducer of type TD342 (Kongsberg) is pointing horizontally towards the receiver 1 m below the surface in 2 m water depth. The vertical directivity pattern is as shown in Fig. 2 with an opening angle of approximately 35 degrees. The horisontal directivity pattern is the same as in the vertical plane. The bandwidth used is 4 kHz centered at 31.25 kHz,

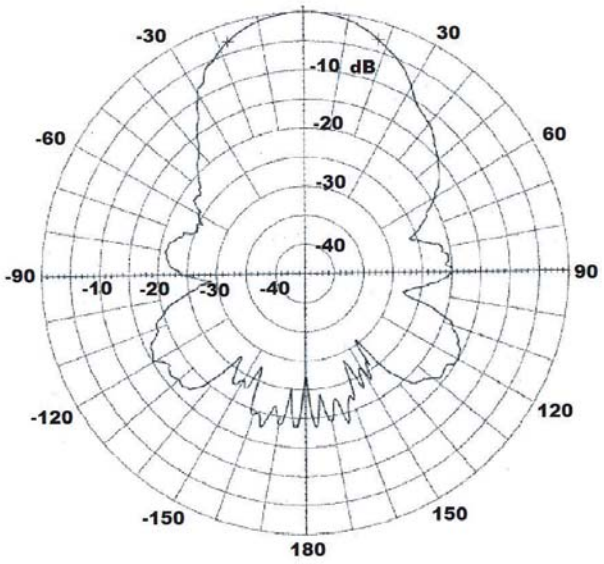

Fig. 2. Transducer directivity pattern, circularly symmetric in the verical plane normal to the beam pattern

and the electrical transmit power approximately 50 W. The transmit source level is 202 dB re 1 μPa and the receiver sensitivity is -180 dBV/μPa.

The wet end, consisting of the transducer and housing, is attached to a standard D/A card in a PC. The PC contains files with encoded and modulated payload data packets.

B. Receive side

The receiver wet end is mounted in the same way as the transmitter, at 2 m below the surface in a water depth of 4 m. The transducer type is identical to the transmitter. The housing contains a 40 dB preamplifier in addition to the transducer. It is connected to an A/D card in a PC. The data are sampled continuously with 12 bit at 250 kHz to the PC for off-line receive processing.

C. Transmitted signal format

During the experiments, data packets of 675 ms are transmitted every 9th second. Each data packet contains 2811 PSK symbols at a rate of 4,2 ksymbols/second. Approximately 70% of these symbols contain data bits. The remaining 30% are used for synchronization and channel estimation, interspersed throughout the block as shown in Fig. 3. The data symbols are modulated by 4-PSK or 8-PSK, with the bit-to-symbol mapping being natural (binary counting round the

circle) or Gray. The transmitted modulation format alternates between the four combinations for each data packet, with the choice of initial synchronization sequence identifying which specific format is used. In this paper we present results only for the Gray mappings (4- and 8-PSK), which turn out to have better overall performance than natural mappings also when using turbo equalization (see [16] for further discussion on this topic). The 4-PSK Gray mapping is (counter-clockwise around the unit circle) 00, 01, 11, 10, while the 8-PSK Gray mapping is 001, 000, 010, 011, 111, 110, 100, 101.

Fig. 3. Transmitted frame format. Hatching denotes synchronization sequences.

The information data bits are protected by a rate-1/2 memory-3 convolutional ECC, with generator polynomials x^3+x^2+x+1 and x^3+x+1. The resulting code bits are permuted using an S-random interleaver before being mapped onto the signal constellation. The total number of information data bits transmitted in a 675-ms packet is approximately 2 kbit for 4-PSK and 3 kbit for 8-PSK, corresponding to information data rates of about 3 kbps and 4,5 kbps, respectively.

III. Environment

The most important environmental parameters are monitored during some of the experiments. Tab. I shows the dates when sound speed profile (SSP) and surface wind speed are measured. The wind speed is measured every 15 minutes. Fig. 4 shows the measured values for the June 16. experiment.

Highly variable conditions should be expected for a series of experiments extending three months. In addition, the wind conditions may change rapidly during a single experiment, as seen in Fig. 4. The SSP is measured during roughly half of the experiments at three locations along the transmission path. A measurement from May 4th is shown in Fig. 5, suggesting a weak surface channel and a more pronounced channel closer to the bottom.

Fig. 6 shows all available SSP's taken at midrange. The local variations around the TX/RX depth are sufficient to create many different communication channels. Raytrace of all the channels has been carried out, and shows that the communication channel is highly variable in terms of multipath structure. There are both minimum and mixed phase channels. Examples of ray arrivals

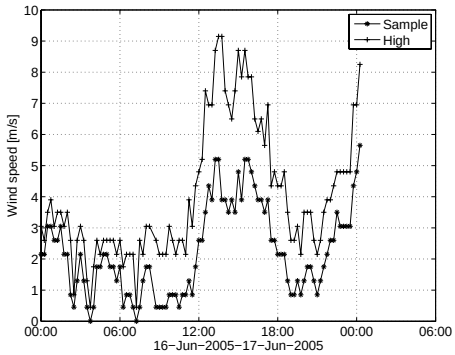

Fig. 4. Wind speed measurements from one of the experiments. Sample values at 15 minute intervals, and high values during the same intervals.

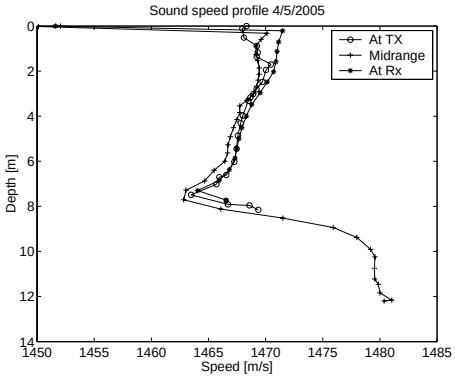

Fig. 5. SSP from May 4th. Measurements at RX, midrange and TX suggesting weak surface duct and a sound channel at 8 m depth.

are direct line of sight, multiple surface bounce rays, multiple bottom bounce rays and mixed surface–bottom bounce rays with a variable number of bounces. An example raytrace taken from May 12th is shown in Fig. 7. This is an example of multipath consisting of a direct ray and several surface–bottom refracted rays. These rays may be attenuated, scattered and Doppler spread, depending on the exact surface conditions. The raytrace used is range independent, and Fig. 7 shows results with RX at 2m depth using the midrange profile, see also example in Fig. 5.

IV. Campaign overview

Each experiment, conducted at the dates shown in Tab. I, lasted for 7 hours. In addition to wind speed and SSP, measurements of precipitation, air temperature, air pressure and wind direction

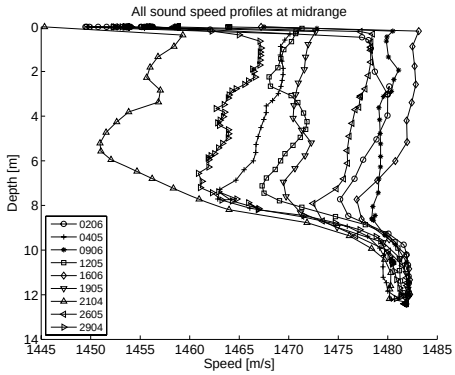

Fig. 6. SSP's from 9 of the experiments. Midrange measurements.

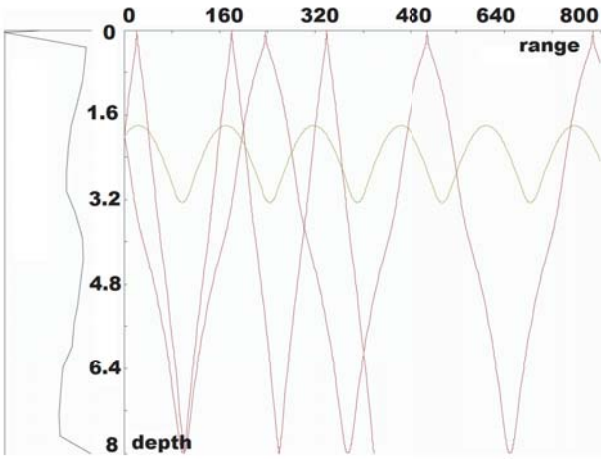

Fig. 7. Raytrace from May 12th. Direct path and a number of surface–bottom refracted rays.

are also carried out, but not used for analysis in this paper. The total number of experiments is 15, approximately once a week during the period March 15th – June 16th 2005.

Fig. 8 gives an overview of the entire measurement campaign, where single values have been extracted for each 7-hour measurement period. The left-hand plots summarize channel conditions and environmental parameters, while the right-hand plots summarize the performance using the receiver structures described in Sec. V.

The CIR length is based on the matched filter CIR estimate, and defined as the difference in delay between CIR coefficients 10 dB or less below the strongest coefficient. The upper left panel shows median values for each measurement period of this 10 dB CIR length, which varies

Dette er en postprint-versjon / This is a postprint version.
DOI til publisert versjon / DOI to published version: 10.1109/JOE.2008.925893

Experiment dates
15/3 29/3 5/4 6/4 13/4 21/4 29/4*
4/5*+ 12/5*+ 19/5*+ 25/5, 26/5*+ 2/6*+ 9/6*+ 16/6*+

TABLE I

DATES FOR THE EXPERIMENTS. *: SSP AVAILABLE. +: WIND SPEED AVAILABLE.

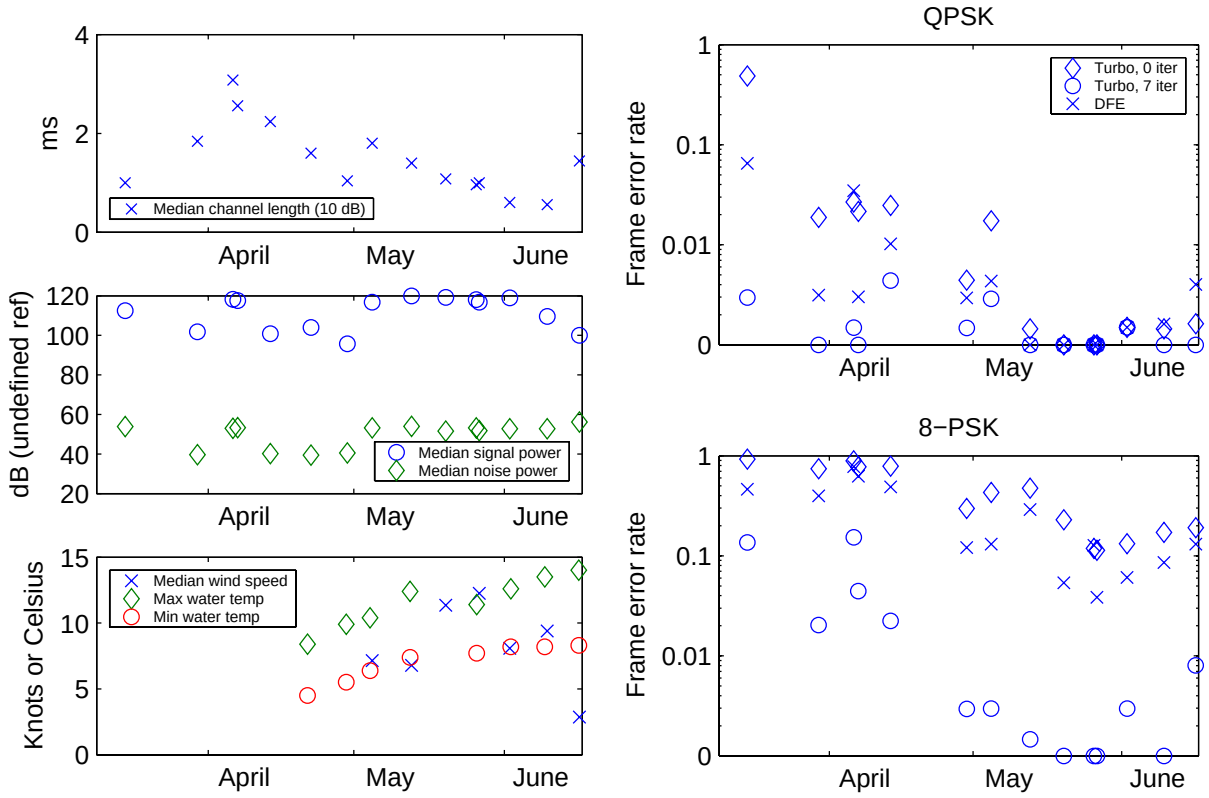

Fig. 8. Overview of measurement campaign, with single values extracted from each measurement day. Upper left: 10dB CIR length (median). Middle left: Signal and noise levels. Lower left: Wind speed and water temperature. Upper right: 4-PSK frame error rate. Lower right: 8-PSK frame error rate.

Dette er en postprint-versjon / This is a postprint version.
DOI til publisert versjon / DOI to published version: 10.1109/JOE.2008.925893

between 0,5 and 3,5 ms. The 30 dB CIR length (not shown) estimated from the reverberation after the end of each packet varies between 60 and 100 ms.

The median signal to noise ratio (SNR) is larger than 40 dB on all measurement days, indicating that the communication system is mostly reverberation-limited. The reverberation is assumed to be the in–plane scattering from the surface and bottom. There are no known strong scatterers in the horisontal plane. The 20 dB drop in signal as well as noise level in April is related to a non-catastrophic equipment malfunction, while the drop in signal (and not noise) level in June is a real effect.

There is a weak trend showing shorter impulse responses towards summer as the water heats up. The exception is the last measurement day of June 16th, where an increase in CIR length is accompanied by weaker received signal.

We use the frame error rate (FER) as measure for the receiver performance averaged over entire 7-hour periods. The FER is defined as the fraction of 675-ms data packets containing one or more bit errors output from the ECC decoder. This is deemed more informative than the bit error rate (BER), which is heavily dominated by the worst conditions encountered during the 7-hour period.

We use the same receiver parameters throughout the entire campaign: The length of the CIR estimate output from the LMS tracker and used in the equalizer is $M = 14$ symbol intervals. The equalizer filter length is $N = 41$ symbol intervals when using turbo equalization, and 21 feedforward symbols and 20 feedback symbols when using a decision feedback equalizer (DFE). Both receivers are based on time-varying channel estimates rather than direct adaptation. The LMS algorithm for the channel tracker uses a step size of 0.03.

As expected, the turbo equalizer performs better than the DFE. The price to pay for this is increased computational complexity in the receiver, due to the number of iterations as well as slightly more complicated equalization and decoding algorithms. When using 4-PSK, the maximum frame error rate (over a 7-hour period) is 6.5% with the DFE-based receiver and 0.3% with turbo equalization. For 8-PSK, the corresponding numbers are 78% with DFE and 13.6% with turbo equalization.

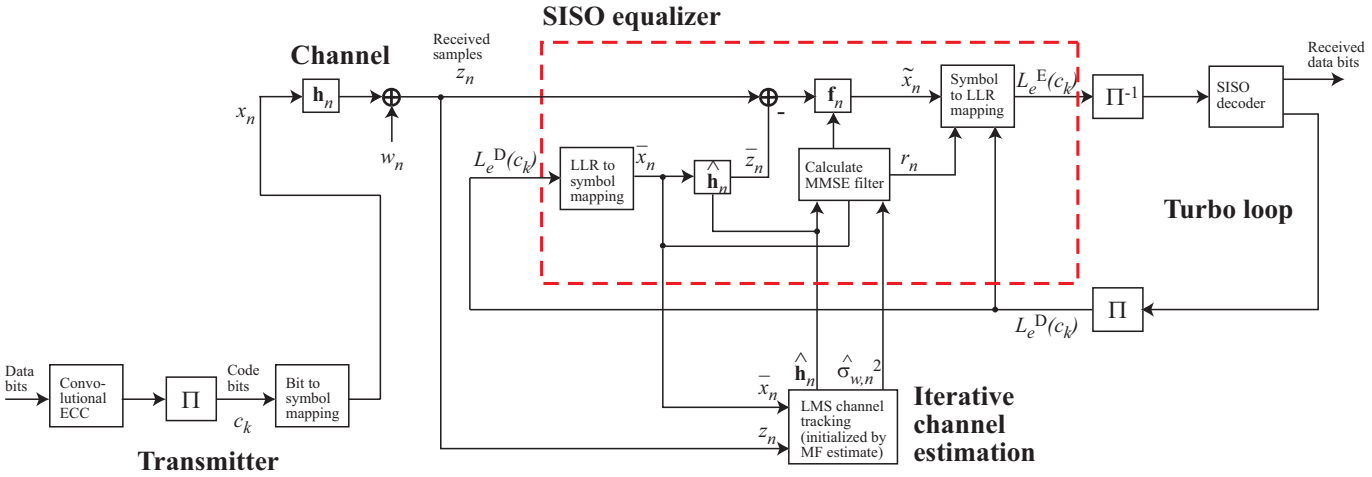

Fig. 9. Principle of linear MMSE turbo equalization with iterative channel estimation. Π and Π^{-1} denote interleaver and deinterleaver, respectively. $\mathbf{h}_n$ and $\mathbf{f}_n$ is channel impulse response and linear equalizer filter, respectively, at symbol interval n. Delay elements and other subtleties are not shown.

V. Receiver structures

A. Preprocessing and synchronization

The first step in the off-line receiver processing, giving the results in Fig. 8, is down-conversion to complex baseband. The baseband signal is downsampled to 6 samples/symbol and cross-correlated with the four different synchronization sequences, to identify the start of each data packet, the modulation format and the initial CIR estimate. The time synchronization criterion is to maximize the energy in a window covering M symbol intervals, corresponding to the length of the CIR estimate output by the channel tracker and used by the equalization algorithm.

The average Doppler shift is estimated and removed. The resulting complex baseband packet along with the initial CIR estimate is further downsampled to two samples/symbol and passed on to one of two receiver structures, either turbo equalization or DFE.

B. Turbo equalization

We use a receiver structure based on turbo equalization as shown in Fig. 9. It was originally developed for ionospheric high frequency (HF, 3-30 MHz) radio communications [17], [18],

and extended to operate on two samples/symbol as described in [19]. The receiver operation is summarized below. For implementation details, please see the references.

The SISO equalizer is based on linear filtering as described in [4], [20], [21]. After 0th iteration (first-time equalization and decoding), the SISO equalizer uses the log likelihood ratios (LLR's) (soft information) fed back from the decoder to compute expected values (means) of each transmitted symbol. For the known training symbols the mean is equal to the symbol itself. These means are passed through a filter with impulse response equal to the estimated CIR yielding the expected values of the received symbols at the output. The symbol mean and variance are estimated for each iteration. These estimates are influenced by the channel noise statistics, see Section VII-D. The mean estimates are subtracted from the received symbols ("soft ISI cancellation") and the remaining signal is passed through a linear filter. The coefficients of this length N filter are calculated based on an estimated length M time-varying CIR and noise variance, using the minimum mean squared error (MMSE) criterion. Due to the means varying with time and iteration number, the filter coefficients are recomputed at each symbol interval and iteration, which can be done recursively [19]–[21]. Finally, the symbols at the filter output are converted back to LLR's by assuming a Gaussian distribution on the equalized symbols. However, the extensive sea trial data suggests that a more accurate probability density function (PDF) than the Gaussian might be a heavy tailed distribution like the normal inverse Gaussian (see Sec. VII).

It should be noted that after 0th iteration, our turbo equalization-based receiver can be expected to perform worse than a DFE-based receiver. This is because the chosen SISO equalizer in this case is a plain MMSE linear equalizer. However, after a few iterations it outperforms the non-iterative DFE-based receiver. This holds true both for reverberation- and noise-limited data sets, verified (but not illustrated here) also for the DFE-based receiver by adding real or Gaussian noise as in Sec. VI.

We have also included channel estimation into the iterative process, using an LMS-based channel tracker. When data symbols have been transmitted, soft symbols (the expected value estimates of each transmitted symbol) $\bar{x}_n$ fed back from the decoder from the previous iteration are used as reference symbols to the tracker.

C. Decision feedback equalization

For comparison, we have also implemented a DFE-based receiver structure, consisting of a DFE followed by a deinterleaver and decoder for the ECC. The CIR at each symbol interval is estimated using linear interpolation between matched filter estimates from the five training sequences, and used to calculate the MMSE-optimal DFE coefficients at each symbol interval.

VI. Case studies on receiver performance

In this section, we investigate in detail the receiver performance on selected measurement days, typical of results observed in different parts of the campaign.

Fig. 10 shows the bit and frame error rate performance (at the ECC decoder output) throughout two measurement days, using 8-PSK signalling. Similar 4-PSK plots are not included as they contain little information due to low error rates. Estimated signal-to-noise ratios and CIR lengths are also shown. Note that the relatively long impulse responses (above 3 ms) on April 6th-7th come together with high bit error rates (and frame error rate close to 1) after the 0th iteration. Two iterations improve the situation significantly, and after 7 iterations most data packets are error-free. The DFE performance is between 0 and 1 iteration of turbo equalization. On May 25th, impulse responses are shorter, mostly below 2 ms, and appear to vary less. On this day, turbo equalization error rates are down to zero after a single iteration (two times equalization and decoding). In these channel conditions the DFE performance is close to turbo equalization with 0 iterations.

Throughout the campaign can be found cases of very stable channel conditions as well as cases of severe variations throughout a packet. We find that the measurements from March 14th-15th stand out as having the most severe variations, and from Fig. 8 we note that this is were turbo equalization most clearly outperform DFE. In Fig. 11 is shown the variations in CIR throughout two example packets on different dates, as estimated by the LMS channel tracker after convergence of the turbo receiver (i.e., using the transmitted training *and* data symbols as reference signal). The left-hand packet has two dominant propagation paths and severe variations throughout the packet, while the right-hand packet has four propagation paths within the tracker window, of which only the weaker two show noticeable variations.

To assess the turbo receiver performance for noise-limited conditions, we have also added artificial noise before running the receiver algorithms. We compare the cases of white Gaussian

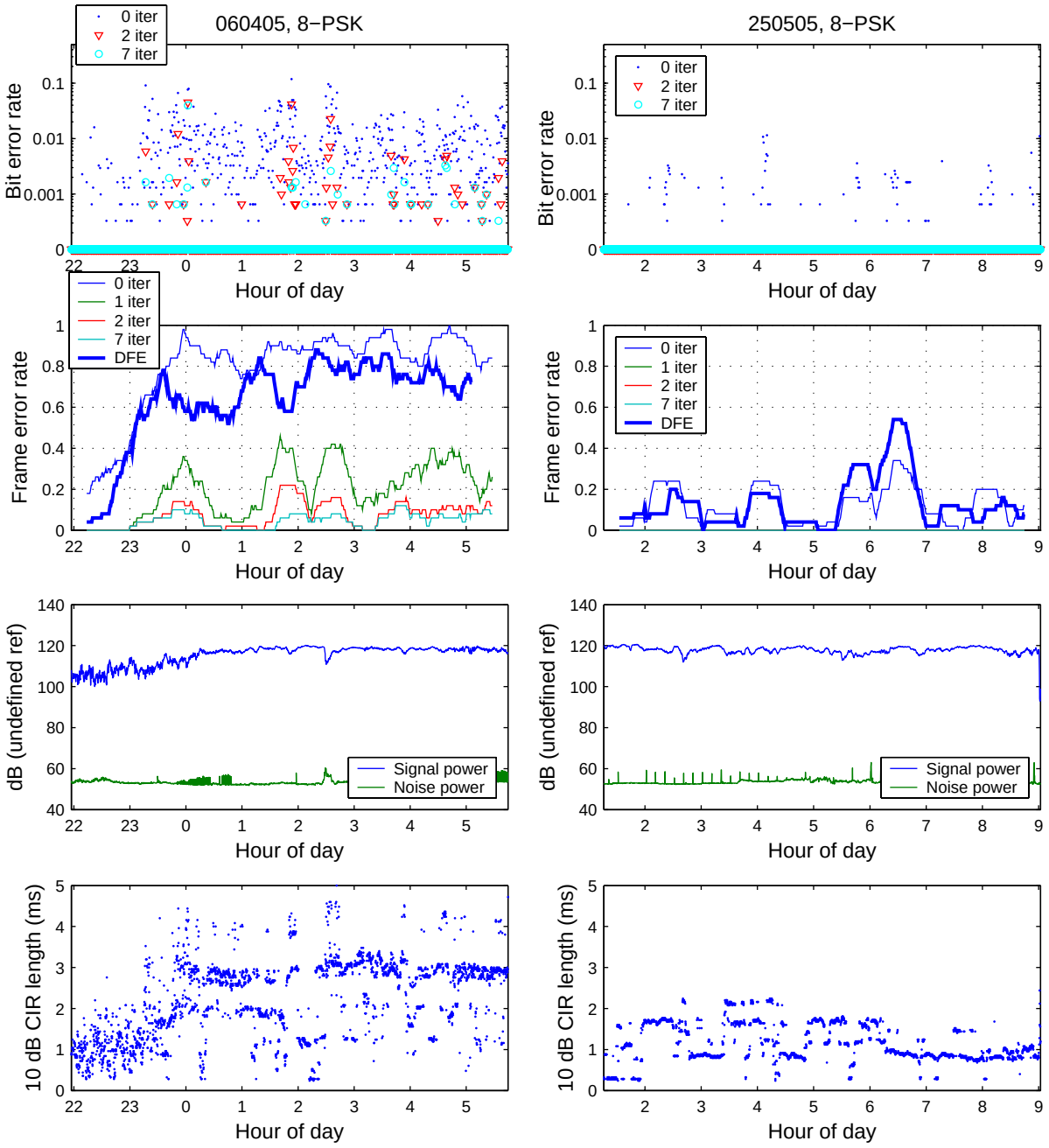

Fig. 10. Performance throughout two measurement days, April 6th-7th (left) and May 25th (right). From top to bottom: (1) Bit error rate in each 8-PSK packet, (2) Frame error rate for 8-PSK using a 50-packet moving average window, (3) Signal and noise level, (4) Estimated CIR length (10 dB below strongest tap).

Dette er en postprint-versjon / This is a postprint version.
DOI til publisert versjon / DOI to published version: 10.1109/JOE.2008.925893

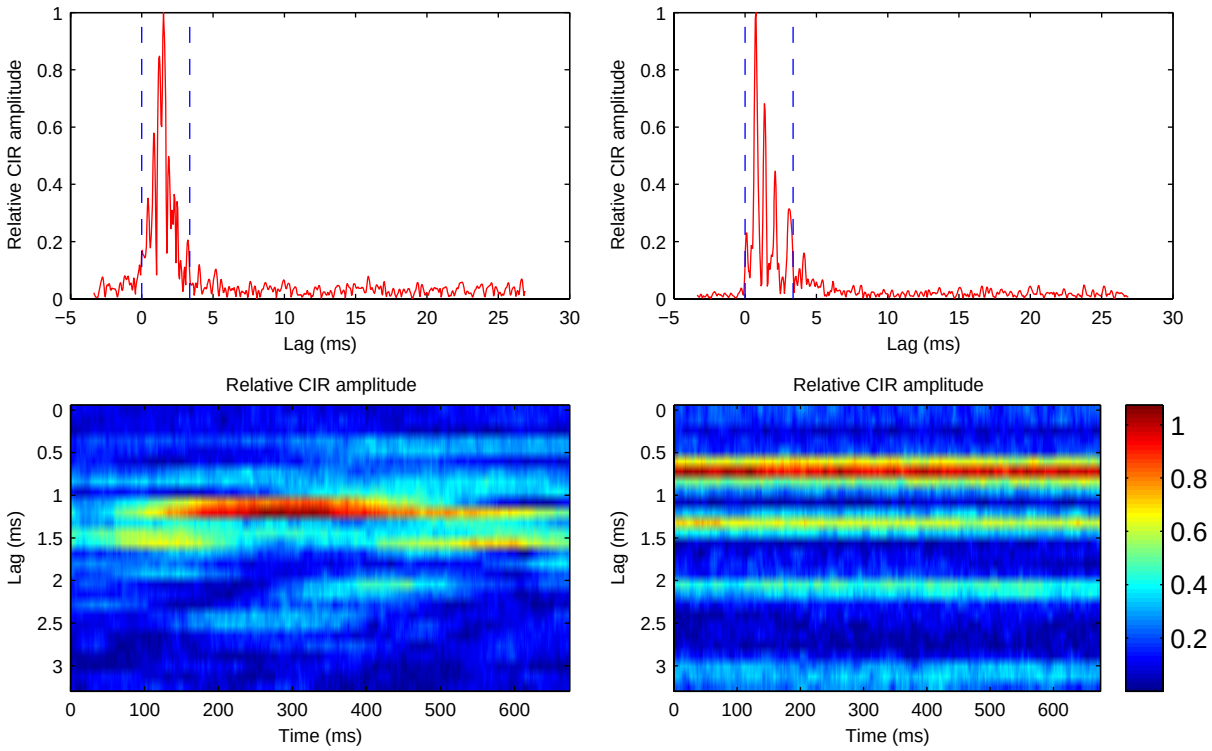

Fig. 11. CIR during two example data packets, on March 14th at 19:48 (left) and on April 7th at 05:01 (right). Upper plots show matched filter CIR estimate based on initial training sequence, with vertical lines indicating the window considered by the channel tracker. Lower plots show CIR amplitude variations as estimated by the LMS channel tracker throughout the packet.

noise and amplified version of real channel noise (recorded after the reverberation interval at the end of the block). Fig. 12 shows the resulting bit error rates (upper panel) and frame error rates (lower panel) for 4-PSK as function of SNR, averaged over 7 hours, for two measurement days. On April 6th-7th, the curves are parallel with an SNR difference of about 1 dB regardless of the number of iterations, and after 5 iterations error rates are reasonably low at SNRs above 10 dB. On May 25th, the curves are parallel after first-time equalization and decoding, while after a number of iterations bit error rates fall off quicker with Gaussian noise than with real noise. With real noise, there is negligible gain from 1 to 5 iterations. After 5 iterations with Gaussian noise, there are no errors at an SNR of 9 dB and higher. The difference between the noise types on May 25th may be due to the real noise being more heavy-tailed than the Gaussian assumption used in the turbo receiver, as discussed in Sec. VII. The longer impulse responses on April 6th-7th may cause the system to be reverberation-limited even at an SNR of 10 dB

Dette er en postprint-versjon / This is a postprint version.
DOI til publisert versjon / DOI to published version: 10.1109/JOE.2008.925893

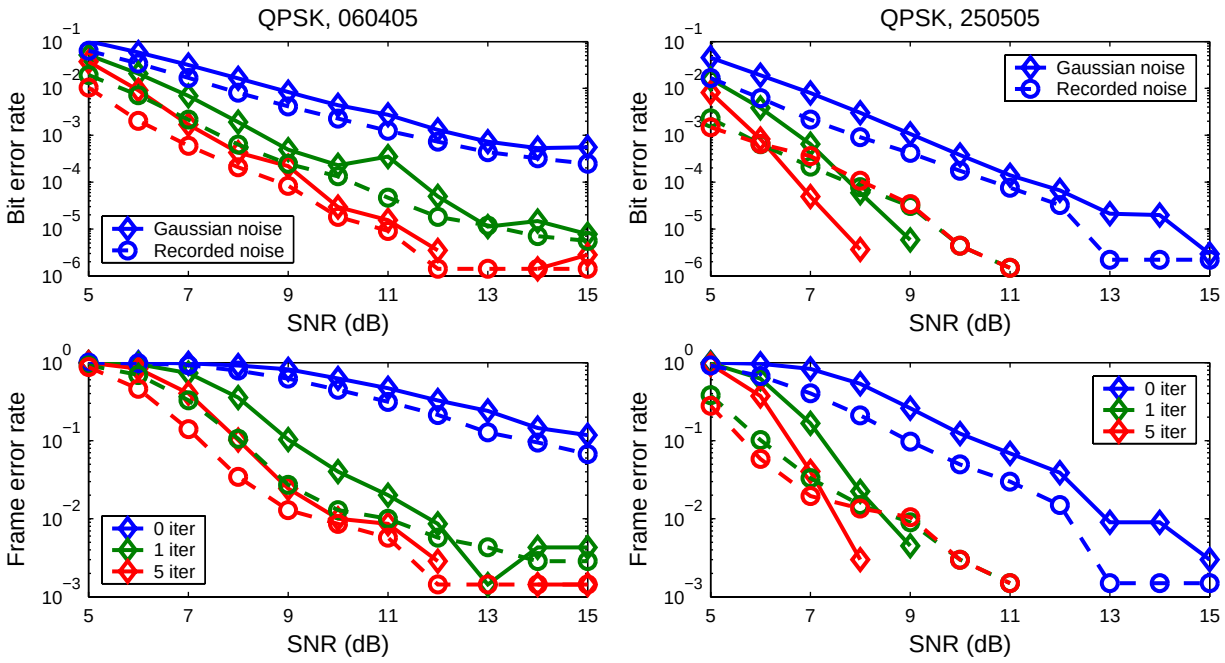

Fig. 12. 4-PSK performance at output of ECC decoder as function of SNR when noise is added, averaged over all data packets recorded on April 6th-7th (left) and May 25th (right). SNR is defined as E_s/N_0 for white Gaussian noise (solid lines), and as E_s/E_n when adding scaled version of noise recorded about 1 sec after end of block (dashed lines). Here, E_s is signal energy per symbol interval, E_n is noise energy per symbol interval, and N_0 is noise spectral density (for white noise, we have $E_n = N_0$). Missing data points indicate zero errors.

(the length of the CIR estimate used in the receiver is 3,4 ms, while we note from Fig. 10 that the 10 dB CIR length is above 4 ms for some of the blocks). Thus the noise statistics are of less importance on April 6-7th than on May 25th.

VII. Turbo receiver performance analysis

The turbo receiver of Fig. 9 constitutes a closed loop system. The aim of this section is to provide further insight into some of the individual blocks of the turbo loop. This problem is also adressed elsewhere [22]. In Section VII-A, VII-B and VII-C we analyze the mapping from soft symbol estimate to LLR under NIG noise assumption, elaborating on the impact of NIG noise in Section VII-E and VII-F. In Section VII-D we generalize the expression for the soft symbol estimates that are fed back in the turbo loop. In Section VII-G we discuss the characteristics of SISO decoders.

Dette er en postprint-versjon / This is a postprint version.
DOI til publisert versjon / DOI to published version: 10.1109/JOE.2008.925893

A. Noise analysis

The channel noise may deviate from the common assumption of Gaussian statistics. In this section we discuss some effects of such a deviation. This discussion is most pertinent to the case where a scaled version of channel noise has been added to the received signal, since the channel without added noise is reverberation-limited. The problem has been addressed in different contexts elsewhere [23]–[28] mostly concerning turbo decoders. A study of turbo receivers supported by extensive sea trials is not known to the authors.

The duty cycle of the acoustic experiments is below 10 %, thus there are large amounts of data available for noise analysis. The data collected during the time intervals without signal are used to estimate the noise statistics. Computation of the sample autocorrelation function over all experiments shows that the noise is white within the receiver bandwidth. The noise PDF is estimated by making histograms of the received noise samples, and this section is devoted to the analysis of the noise PDF. The NIG density [29] may be used to model non–Gaussian data with heavy–tailed statistics. The introduction of this density is motivated by similar applications [30], [31]. The symmetric NIG PDF for a real-valued random variable is [32]

$$\begin{aligned} p_X(x) &= \frac{\alpha\delta}{\pi}\frac{e^{\alpha\delta}}{q(x)}K_1(\alpha q(x)) \\ q(x) &= \sqrt{(x-\mu)^2+\delta^2} \end{aligned} \tag{1}$$

where α and δ are parameters, μ is the mean, and $K_1(\cdot)$ is the modified Bessel function of the second kind and first order. An alternative parametrization is given by defining [29]

$$\sigma^2 = \frac{\delta}{\alpha} \tag{2}$$

$$\bar{\alpha} = \alpha\delta \tag{3}$$

where σ^2 is the variance and the shape parameter $\bar{\alpha}$ is location- and scale-invariant. We write $X \sim \text{NIG}(\mu, \sigma^2, \bar{\alpha})$ to indicate a symmetric NIG distributed random variable with the parameters defined above. In the limit as $\bar{\alpha}$ gets large, the NIG PDF becomes Gaussian, while smaller values of $\bar{\alpha}$ corresponds to heavier tails. For plots of the NIG PDF for different values of $\bar{\alpha}$, we refer to [31].

A mean value of $\mu = 0$ is the best fit to noise measurements. $\bar{\alpha}$ is determined by a curve fit to the measured noise PDF, using a quadratic cost function (the mean-squared error between measured and NIG PDF is minimized). Fig. 13 shows the noise PDF for four of the days. Each

Dette er en postprint-versjon / This is a postprint version.
DOI til publisert versjon / DOI to published version: 10.1109/JOE.2008.925893

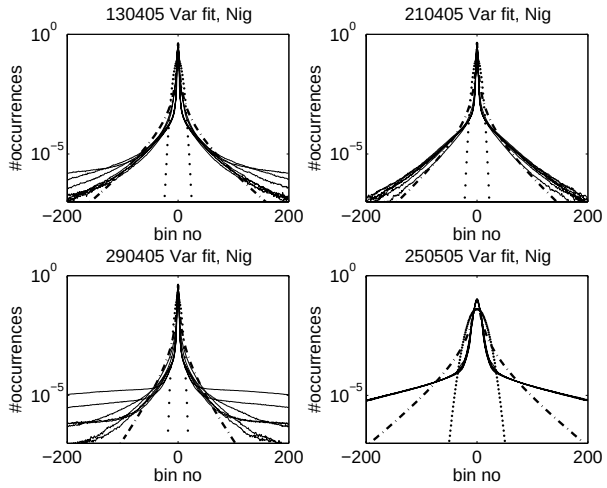

Fig. 13. Noise probability density function estimates based on 1/2 hour of noise data (thin lines). Equal variance Gauss fit (dotted) and NIG fit (dash–dot), with parameter $\bar{\alpha}$ as follows: 130405: $\bar{\alpha} = 0.030$. 210405: $\bar{\alpha} = 0.031$. 290405: $\bar{\alpha} = 0.055$. 250505: $\bar{\alpha} = 0.133$.

plot contains a number of PDF estimates, where each estimate is made up of 1/2 hour of data, containing the real part of the noise samples. The dash–dot line is a quadratic fit of a NIG density. The dotted line is a Gaussian PDF with its mean and variance equal to the estimates from the noise measurements. PDF fits with Cauchy and Laplace PDF's are also performed, but not shown here because the NIG fit is found to be much better. It is evident from Fig. 13 that the NIG is a much closer fit than the Gaussian, and this goes for all of the experiments.

Complex-valued heavy-tailed noise may be modelled as a two-dimensional MNIG (multivariate NIG) pdf, which is circularly symmetric and has uncorrelated but statistically dependent real and imaginary parts. The two-dimensional zero-mean symmetric MNIG pdf with uncorrelated components is given by [31]

$$\begin{aligned} p_X(x_1, x_2) &= \frac{\delta e^{\alpha\delta}}{\sqrt{2}} \left(\frac{\alpha}{\pi q(x_1, x_2)} \right)^{3/2} K_{3/2}(\alpha q(x_1, x_2)) \\ q(x_1, x_2) &= \sqrt{x_1^2 + x_2^2 + \delta^2} \end{aligned} \tag{4}$$

The marginal PDF of each component x_1 and x_2 is NIG-distributed with parameters α and δ [31], hence the PDF estimation method described above is still valid when considering complex-valued signals.

Dette er en postprint-versjon / This is a postprint version.
DOI til publisert versjon / DOI to published version: 10.1109/JOE.2008.925893

B. Analysis of linear SISO equalizer under NIG noise assumption

Here, we analyze the linear SISO equalizer under the assumption of the channel noise samples being iid NIG distributed. For simplicity, we consider the case of BPSK modulation and real-valued channel noise w_n, a known and constant channel impulse response, and symbol-spaced sampling input to the equalizer filter.

With reference to Fig. 9 we denote the constant channel impulse response as $\mathbf{h}_n = \mathbf{h}$, covering lags in the range $[0, M-1]$. Due to the known channel assumption we have $\hat{\mathbf{h}} = \mathbf{h}$. The input LLRs $L_e^D(c_k)$ are denoted L_n (due to BPSK modulation, we have one bit/symbols and $k = n$). The equalizer filter $\mathbf{f}_n$ covers lags in the range $[-N_1, N_2]$.

Define $\mathbf{g}_n$ as the convolution of $\mathbf{h}$ and $\mathbf{f}_n$. $\mathbf{g}_n$ will cover lags in the range $[-N_1, N_2 + M - 1]$. Further, define the vectors

$$\mathbf{x}_n = [x_{n+N_1} \ \ldots \ x_{n+1} \ x_n \ x_{n-1} \ \ldots x_{n-N_2-M+1}]^T \tag{5}$$

$$\mathbf{x}'_n = [x_{n+N_1} \ \ldots \ x_{n+1} \ 0 \ x_{n-1} \ \ldots x_{n-N_2-M+1}]^T \tag{6}$$

$$\bar{\mathbf{x}}'_n = [\bar{x}_{n+N_1} \ \ldots \ \bar{x}_{n+1} \ 0 \ \bar{x}_{n-1} \ \ldots \bar{x}_{n-N_2-M+1}]^T \tag{7}$$

$$\mathbf{w}_n = [w_{n+N_1} \ \ldots \ w_{n+1} \ w_n \ w_{n-1} \ \ldots w_{n-N_2}]^T \tag{8}$$

In the definition of the vector $\bar{\mathbf{x}}'_n$ of *a priori* means, the element $\bar{x}_n$ is replaced by zero when computing the symbol estimate $\tilde{x}_n$. This important subtlety, which is not captured by Fig. 9, is essential to the operation of linear turbo equalization [20]. We also define $d_n = x_n - \bar{x}_n$ and $\bar{\mathbf{d}}'_n = \mathbf{x}'_n - \bar{\mathbf{x}}'_n$.

The symbol estimate $\tilde{x}_n$ is given by

$$\begin{aligned} \tilde{x}_n &= \mathbf{g}_n^H \mathbf{x}_n - \mathbf{g}_n^H \bar{\mathbf{x}}'_n + \mathbf{f}_n^H \mathbf{w}_n \\ &= g_0(n) x_n + \mathbf{g}_n^H \bar{\mathbf{d}}'_n + \mathbf{f}_n^H \mathbf{w}_n \end{aligned} \tag{9}$$

where $g_0(n)$ is the element of $\mathbf{g}_n$ corresponding to zero lag. In (9), $g_0(n)x_n$ is the desired output, $\mathbf{g}_n^H \bar{\mathbf{d}}'_n = \mathbf{g}_n^H (\mathbf{x}'_n - \bar{\mathbf{x}}'_n)$ is the residual ISI term, and $\mathbf{f}_n^H \mathbf{w}_n$ is the filtered channel noise.

The weighted sum of iid NIG random variables follows a heavy-tailed distribution which is not exactly NIG unless all weights are equal [33]. However, a close match (differing only in sixth and higher order moments) can be found by matching the second and fourth order moment, which gives

$$\mathbf{f}_n^H \mathbf{w}_n \sim \text{NIG}\left(0, \ \mathbf{f}_n^H \mathbf{f}_n \sigma_w^2, \ \frac{(\mathbf{f}_n^H \mathbf{f}_n)^2}{\sum_i (f_{n,i}^* f_{n,i})^2} \bar{\alpha}_w\right) \tag{10}$$

Dette er en postprint-versjon / This is a postprint version.
DOI til publisert versjon / DOI to published version: 10.1109/JOE.2008.925893

where σ_w and $\bar{\alpha}_w$ are the NIG parameters of a single channel noise sample.

Let us first consider the case of a converged turbo equalizer with large and error-free input LLRs, in which case we have perfect ISI cancellation due to $\bar{\mathbf{x}}'_n = \mathbf{x}'_n$. Then, the PDF of $\tilde{x}_n$ will be approximately NIG with $\mu = g_0 x_n$ and other parameters as shown in (10). This will also be the case for a DFE with error-free feedback, provided that precursor ISI can be neglected. We also note that for a converged turbo equalizer with perfect feedback, the MMSE-optimal equalizer filter is identical to the channel matched filter multiplied by a scaling factor [4], hence $\mathbf{f}_n$ can be replaced by $K\mathbf{h}$ in the expressions for NIG parameters in (10), where K is a scaling factor. Note that $\bar{\alpha}$ is independent of K.

Let us then consider earlier iterations, when the input LLRs are not large, such that $\bar{x}_n \neq x_n$. In this case, it can be shown that the PDF of the residual ISI $d_n = x_n - \bar{x}_n$ can take on a variety of shapes (depending on the magnitude of the LLRs fed back from the previous iteration), with the one thing in common that d_n is bounded by $< -2, +2 >$. Hence, the PDF of the residual ISI term $\mathbf{g}_n^H \bar{\mathbf{d}}'_n$ will also be bounded, and the overall PDF of $\tilde{x}_n$ will be a convolution of a NIG PDF and a bounded PDF, with tail behavior governed by the NIG contribution.

C. Demapping to LLRs

For a turbo receiver to operate optimally, it is essential that the LLRs represent as correct likelihood information as possible. In this regard, the computation of LLRs from symbol estimates ("symbol-to-LLR demapping") should be based on the actual conditional PDFs of the symbol estimates. In practice, however, the symbol estimate PDF's throughout the iterations will take on a variety of shapes, which cannot be described by simple analytical expressions.

In linear turbo equalization with MMSE-optimal equalizer filter, it can be shown [20] that the conditional mean and variance of the symbol estimates $\tilde{x}_n$ are $\mu_{\tilde{x}} = g_0 x_n$ and $\sigma^2_{\tilde{x}} = g_0 - g_0^2$. The symbol-to-LLR demapper generally used in linear turbo equalization assumes at all iterations the conditional PDF of $\tilde{x}_n$ to be Gaussian with these parameters. Note that in the case of Gaussian channel noise, the Gaussian assumption is correct for a converged turbo equalizer with perfect feedback, but an approximation at early iterations. For BPSK, the resulting demapper function is a straight line and the pdf of output LLRs is a scaled version of the pdf of $\tilde{x}_n$ [20]:

$$l_G(\tilde{x}_i) \quad = \quad \frac{2\tilde{x}_i}{1 - g_0} \tag{11}$$

Dette er en postprint-versjon / This is a postprint version.
DOI til publisert versjon / DOI to published version: 10.1109/JOE.2008.925893

If the channel noise samples are iid NIG distributed, the conditional PDF for a converged turbo equalizer are approximately NIG distributed with the parameter $\bar{\alpha}_{\tilde{x}}$ given by (10). Also at earlier iterations the PDF will be heavy-tailed with tail behavior governed by the NIG contribution. Hence, we argue that a symbol-to-LLR demapper derived from the NIG PDF should be applied. For BPSK (considering real-valued noise only), the resulting demapper function is described by

$$\begin{aligned} l_N(\tilde{x}_i) &= \ln\{\frac{q_m}{q_p}\frac{K_1(\alpha q_p)}{K_1(\alpha q_m)}\} \\ q_p &= \sqrt{\delta^2+(\tilde{x}_i-g_0)^2} \\ q_m &= \sqrt{\delta^2+(\tilde{x}_i+g_0)^2} \end{aligned} \tag{12}$$

The expressions of (11) and (12) are shown in Fig. 14 for the Proakis C channel, $\mathbf{h} = [.227\ \ .46\ \ .688\ \ .46\ \ .227]^T$. This channel model is often used for evaluation purposes in communication systems, and we use it in order to produce convenient comparisons. The SNR is set to 10 dB, and $M = 5, N = 10$ are used in order to compute $\mathbf{f}_n$. $\bar{\alpha}, \sigma$ are taken from the NIG fit of April 21th in Fig. 13. (10) is used in the evaluation of (12) in order to get Fig. 14. We

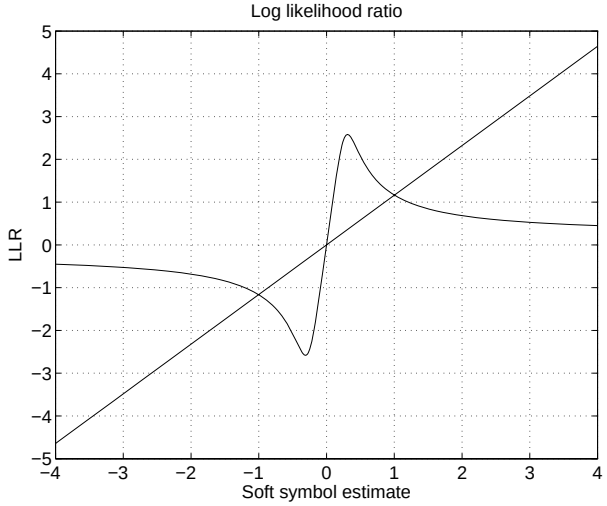

Fig. 14. Log likelihood ratio with Gauss (straight line) and NIG(0,0.36,0.073) noise model

note that the significant deviations occur for large $\tilde{x}_i$, i.e., at the tails of the pdf distributions. In these areas the LLR's are too large in the case of NIG noise and Gaussian demapper, i.e, the input to the SISO decoder is too optimistic with regards to the certainty of a sample $\tilde{x}_i$ with high magnitude. Another way to interpret this is to observe that the NIG demapper contains an

Dette er en postprint-versjon / This is a postprint version.
DOI til publisert versjon / DOI to published version: 10.1109/JOE.2008.925893

outlier detection mechanism: In the case of high magnitudes the likelihood decreases, indicating that this may be from a NIG noise sample. We also note that $l_N(\tilde{x}_i)$ peaks at the expected value of $\tilde{x}_i$ and that the limit as $\tilde{x}_i$ gets large is 2α.

In general too small LLR values (compared to the values representing correct likelihood information) will cause a turbo receiver to converge slower and possibly to a higher final BER, while too large LLR values may cause divergence of the iterative procedure. An example of the latter is described in [34].

For QPSK and higher-order constellations (considering complex-valued noise), the NIG demapper is given by replacing the Gaussian PDF by the two-dimensional MNIG PDF (4) in [20, Eqn. (8)].

In order to obtain further insight we approximate $l_N(\tilde{x}_i)$, see Appendix II. The approximation in (23) and (28) are shown in Fig. 15 together with the asymptotic value of 2α. The pdf of $l_N(x)$

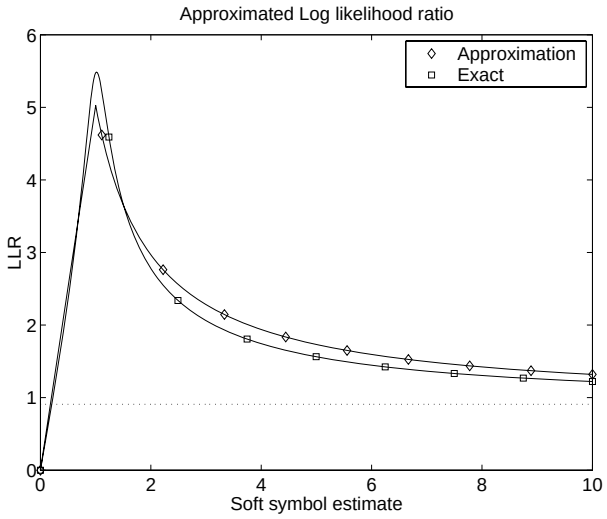

Fig. 15. Approximation to Log likelihood ratio with NIG noise model

is now found [35] by collecting corresponding events in the L and X space to get expressions for the probabilities, and taking the derivative in order to get the pdf. We consider the case were $x_n = 1$, noting that $x_n = -1$ is similar. As seen from Fig. 15 there are two cases:

Dette er en postprint-versjon / This is a postprint version.
DOI til publisert versjon / DOI to published version: 10.1109/JOE.2008.925893

$l < 2\alpha$:

$$\begin{aligned} \Pr(L < l \mid x_n = 1) &= \Pr(X < \frac{l}{\gamma} \mid x_n = 1) \\ p_L(l \mid x_n = 1) &= \frac{d}{dl}\Pr(L < l \mid x_n = 1) = p_X(\frac{l}{\gamma} \mid x_n = 1)\frac{1}{\gamma} \end{aligned} \tag{13}$$

were $p_X(\frac{l}{\gamma} \mid x_n = 1)$ is given by (1) with $\mu = 1$.

$2\alpha < l < \gamma$:

$$\begin{aligned} \Pr(L < l \mid x_n = 1) &= \Pr(X < \frac{l}{\gamma} \mid x_n = 1) + \Pr(X > \frac{\gamma - 2\alpha}{l - 2\alpha} \mid x_n = 1) \\ &= 1 + \Pr(X < \frac{l}{\gamma} \mid x_n = 1) - \Pr(X < \frac{\gamma - 2\alpha}{l - 2\alpha} \mid x_n = 1) \\ p_L(l \mid x_n = 1) &= p_X(\frac{l}{\gamma} \mid x_n = 1)\frac{1}{\gamma} + p_X(\frac{\gamma - 2\alpha}{l - 2\alpha} \mid x_n = 1)\frac{\gamma - 2\alpha}{(l - 2\alpha)^2} \end{aligned} \tag{14}$$

The shape of the pdf in (14) is shown in Fig. 16 together with the corresponding simulated pdf. The simulated PDF error floor at approximately 10^{-3} is believed to come from the limited

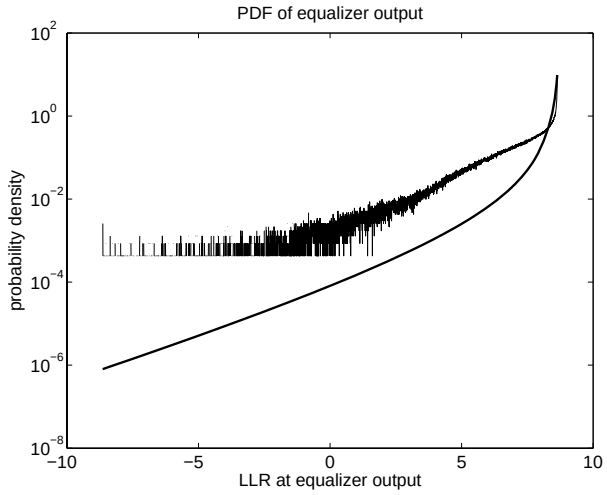

Fig. 16. Empirical and approximate analytic PDF of the equalizer output

number of trials used.

D. Mapping to priors

We now turn to the analysis of the feedback part of the turbo equalizer. Consider the picture in Fig. 9, assuming BPSK modulation. The task is to find an expression for the equalizer output

$\tilde{x}_n$ from the inputs z_n. z_n is the output from the acoustic channel and L_e^D is the feedback LLR from the subsequent SISO decoder shown in Fig. 9. In this context we interpret both inputs as random variables. The PDF on z_n is given by the noise w_n. We will return to the question of the statistics of L_e^D, and for now regard this quantity as a random variable, noting that this approach also is taken by others [36]. The MMSE criterion is to minimize $E[|x_n - \tilde{x}_n|^2]$ with respect to $\tilde{x}_n$. This expectation is to be carried out over both random variables z_n and L_e^D. The cost criterion may be written

$$\begin{aligned} E[|x_n - \tilde{x}_n|^2] &= \int_{\mathbf{w}} \int_l |x_n - \tilde{x}_n|^2 p(\mathbf{w}, l) dl d\mathbf{w} \\ &= \int_l \int_{\mathbf{w}} |x_n - \tilde{x}_n|^2 p(\mathbf{w}|l) d\mathbf{w} p_{L^D}(l) dl \\ &= \int_l E[|x_n - \tilde{x}_n|^2 | L_e^D = l] p_{L^D}(l) dl \end{aligned} \tag{15}$$

where $p(\mathbf{w}, l)$ is the joint PDF on the noise and the LLR, $p(\mathbf{w}|l)$ is the conditional PDF and $p_{L^D}(l)$ is the marginal PDF on the LLR. The minimization of $E[|x_n - \tilde{x}_n|^2 | L_e^D]$ is an MMSE problem where L_e^D is considered known. The solution to this problem, called $\tilde{x}_{n|L_e^D}$, is given in [20]. We use this result for the BPSK signal constellation:

$$\begin{aligned} \tilde{x}_{n|L_e^D} &= E[x_n | L_e^D] + \mathbf{a}_n^H (\mathbf{z}_n - E[\mathbf{z}_n | L_e^D]) \\ \mathbf{a}_n &= R_{\mathbf{zz}}^{-1} R_{\mathbf{z}x} \\ R_{\mathbf{zz}} &= E[\mathbf{z}_n \mathbf{z}_n^H | L_e^D] - E[\mathbf{z}_n | L_e^D] E[\mathbf{z}_n^H | L_e^D] \\ R_{\mathbf{z}x} &= E[\mathbf{z}_n x_n^* | L_e^D] - E[\mathbf{z}_n | L_e^D] E[x_n^* | L_e^D] \end{aligned} \tag{16}$$

By using (15) the linear MMSE estimate is given by

$$\tilde{x}_n = E[\tilde{x}_{n|L_e^D}] = \int_l \tilde{x}_{n|L_e^D = l} p_{L^D}(l) dl \ . \tag{17}$$

This is a generalized result, more closely modelling the receiver of Fig. 9. It requires knowledge of $p_{L^D}(l)$; the PDF of L_e^D.

E. Simulations with NIG-distributed noise

A simulation study is performed, where the channel noise samples are iid NIG distributed (rather than iid Gaussian distributed) with $\bar{\alpha} = 0.03$. The simulation setup is operating at one sample/symbol, using the Proakis C channel. Note that the CIR is constant, and known to the

Dette er en postprint-versjon / This is a postprint version.
DOI til publisert versjon / DOI to published version: 10.1109/JOE.2008.925893

receiver (i.e., channel estimation is not included in the simulation). The ECC and filter lengths are the same as for the measurement results. An S-random interleaver with block size of 65536 code bits is applied, and 200 interleaver blocks are simulated.

The simulation results, shown in Fig. 17, shows that when the channel noise is iid NIG distributed, using a NIG demapper significantly outperforms the Gaussian demapper.

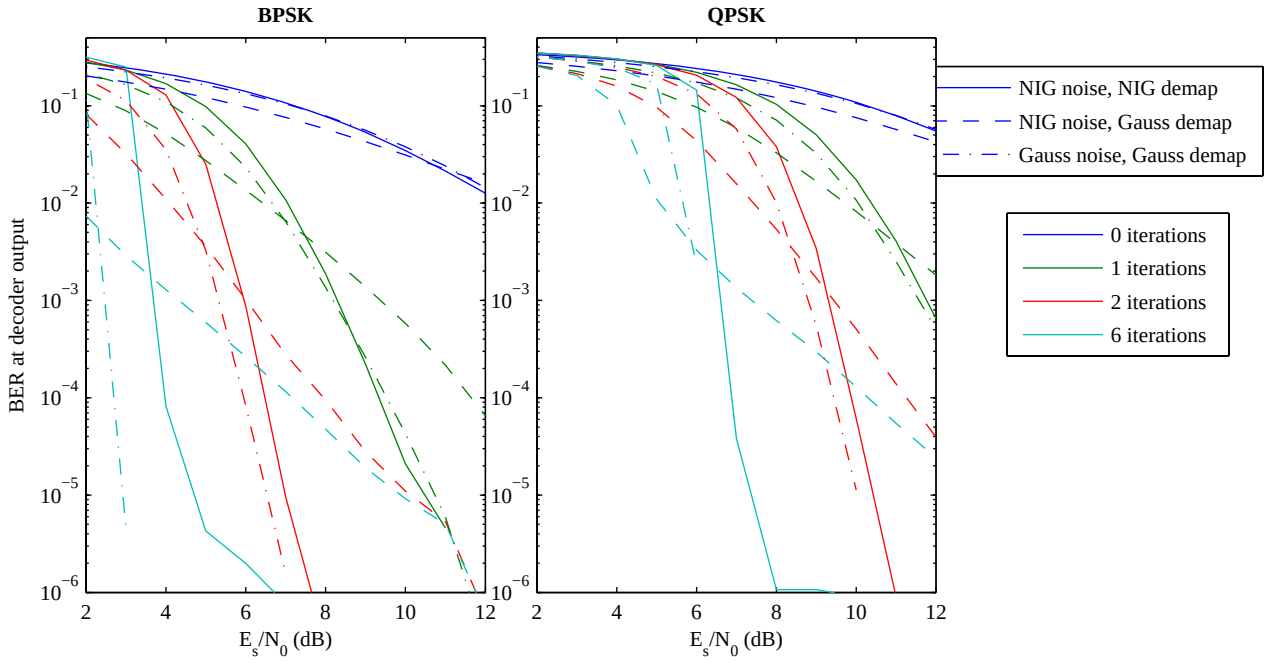

Fig. 17. Simulation results using symbol-to-LLR demappers matched and not matched to channel noise.

F. Using NIG demapper on measurement data

A natural next step is to apply the NIG demapper to the receiver operating on the measurement data. We did this for a number of data sets, and found that in general applying the NIG demapper actually is inferior to the Gaussian demapper (figure not included), requiring approximately 1 dB higher SNR to obtain the same BER and exhibiting a higher error floor.

Hence, there is evidently a discrepancy between theoretical arguments and simulation results on one side, and actual performance on real-world data on the other side. This is likely to be be due to some aspect of the real-world measurement data or the iterative receiver not being properly modelled in the theoretical analysis and simulations. Possible explanations include:

Dette er en postprint-versjon / This is a postprint version.
DOI til publisert versjon / DOI to published version: 10.1109/JOE.2008.925893

- The noise samples may not be statistically independent even though they are uncorrelated (white). This may e.g. be the case for bursty noise, which on small time scales may be close to Gaussian even though the overall PDF is heavy-tailed.
- The NIG PDF fit may not be good enough.
- When operating on real-world channel data, (iterative) channel estimation is part of the receiver. This was not included in the simulations. Channel estimation errors will cause an additional noise contribution on the symbol estimates output from the equalizer, which may be closer to Gaussian than the noise contribution due to channel noise.

G. Decoder soft information statistics

We now turn to the problem of characterizing the statistics of the SISO decoder soft information. The LLR L_e^D is often used for its representation. Thus we pose the following problem: The SISO decoder input are soft symbol estimates $L^E(c_{n,j})$ with known PDF. What can we say about the statistics of the decoder LLR estimate $\hat{L}_e^D$? We omit the interleavers of Fig. 9 in this analysis. Their mission is to ensure independent LLR estimates and we acknowledge this as crucial for the turbo receiver to work well. However, it is not important in this context. We restrict ourselves to discussing only one SISO decoder architecture; the soft output Viterbi algorithm (SOVA) as proposed in [37] (the decoder used in our experiments is the algorithm by Bahl et al. (BCJR) [38], but we argue that similar results should apply). It is assumed that the regular Viterbi algorithm (VA) is known to the reader, see e.g., [39] for a discussion. In our case the VA is used for decoding of a convolutional code. The code may be viewed as a state machine, e.g., with a code of constraint length 3 and BPSK symbol alphabet the number of states is 2^3. The VA works by estimating the most likely sequence of states given the measurements $L^E(c_{n,j})$. The VA output is the output value of the corresponding state. In order to estimate the state sequence a cost function is computed at each stage of the trellis, and accumulated for the survivors of each node in the trellis. In the SOVA this cost function is quadratic:

$$M_m \;=\; \frac{E_S}{N_0} \sum_{n=n_0-\delta}^{n_0} \sum_{j=1}^{Q} |L^E(c_{n,j}) - x_{n,j}^{(m)}|^2, \tag{18}$$

$m = 1, 2$. δ is a decoding delay large enough so that all the survivor paths have merged with high probability, $x_{n,j}^m$ is the j'th bit (out of Q) on the branch of the m'th path at time n. If the acoustic channel noise is Gaussian, the LLR estimate $L^E(c_{n,j})$ is also Gaussian. In this case

Dette er en postprint-versjon / This is a postprint version.
DOI til publisert versjon / DOI to published version: 10.1109/JOE.2008.925893

M_m is a random variable with Chi–square PDF and δQ degrees of freedom: $\chi^2_{\delta Q}$. If the acoustic channel noise is NIG, the LLR estimate $L^E(c_{n,j})$ is also approximately NIG. It is interesting to note that there is a closed form expression for the PDF of M_m in the NIG case as well [40].

In practical systems using the SOVA, the LLR estimate $\hat{L}_e^D$ is approximated with $\Delta = |M_2 - M_1|$. We have not derived the PDF of Δ, but the appendix shows a comparison of these PDF's for the cases of Gaussian and NIG channel noise.

VIII. Conclusions

This paper describes the outcome of an extensive series of underwater acoustic communication experiments. The sea trials extend over a period of three months, and consist of 7 hour contiguous telemetry transmissions approximately once a week. The communication channel is characterized by high SNR, insignificant Doppler and highly variable multipath. The presence of multipath is quantified by raytracing based on SSP's taken during the experiments, and also by impulse response estimates from the transmitted data.

The receiver consists of a channel tracker, an equalizer and a decoder. These units are jointly adapted by means of the turbo principle: They are exchanging soft information in terms of log likelihood ratio estimates, and iterating in order to improve performance.

The telemetry system shows no link outage over the three month period, i.e, there is no period extending several transmission packets where the bit error rate is close to 50%. The maximum frame error rate over any single experiment (7 hour period) is 0.3% with 4-PSK modulation. For reference a DFE receiver is used, and the result is 6.5% maximum frame error rate. For 8-PSK, the corresponding numbers are 13.6% with turbo equalization and 78% with DFE.

Adding scaled recorded or Gaussian noise to selected data sets shows that turbo equalization with 4-PSK modulation performs well down to SNRs of about 10 dB.

Analysis of the noise statistics revealed that the channel noise is heavy-tailed and that its PDF can be approximated by NIG. It was also found that the noise is white within the measurement bandwidth. Further, it was argued that the turbo receiver, and in particular the symbol-to-LLR demapper, should be matched to the actual noise statistics for optimal performance. Simulations showed that when the channel noise samples are i.i.d NIG-distributed, and the CIR is known and constant, using a demapper matched to the NIG PDF significantly outperforms a demapper

Dette er en postprint-versjon / This is a postprint version.
DOI til publisert versjon / DOI to published version: 10.1109/JOE.2008.925893

matched to the Gaussian PDF. This effect is, however, not found to apply to the measurement data.

APPENDIX I
LLR STATISTICS FROM SISO DECODER

This appendix shows one way to proceed in order to find the LLR statistics of a SISO decoder using the SOVA algorithm. We consider two cases: The channel noise is white and 1) Gaussian or 2) NIG. Consider the random variables M_1 and $-M_2$ from (18). Their PDF's are related through

$$p_{-M_2}(m) \;=\; p_{M_1}(-m) \tag{19}$$

and their sum has the PDF

$$\begin{aligned} p_{M_1-M_2}(m) &= \int_x p_{M_1}(x)p_{-M_2}(x-m)dx \\ &= p_{M_1-M_2}(-m) \end{aligned} \tag{20}$$

which is symmetric. In general, for a symmetric PDF $p_{M_1-M_2}(m)$, we have that the PDF of $\Delta = |m|$ is

$$p_\Delta(x) = \begin{cases} 2p_{M_1-M_2}(x) & x \geq 0 \\ 0 & x < 0 \end{cases} \tag{21}$$

Fig. 18 shows significant differences comparing the SOVA LLR estimates with Gauss (right panels) and NIG (left panels) noise. The main difference is, as expected, in the tail of the distributions.

APPENDIX II
LLR STATISTICS FROM NIG DEMAPPER

In this appendix we approximate the NIG LLR. As seen from Fig. 14 there are two regions, and for simplicity we use $g_0 = 1$ and write $\tilde{x}_i = x$. Thus we approximate $l_N(x)$ in the two regions $0 < x < 1$ and $x > 1$:

$$l_N(x) \;=\; \begin{cases} f_1(x) & 0 < x < 1 \\ f_2(x) & x > 1 \end{cases} \tag{22}$$

Dette er en postprint-versjon / This is a postprint version.
DOI til publisert versjon / DOI to published version: 10.1109/JOE.2008.925893

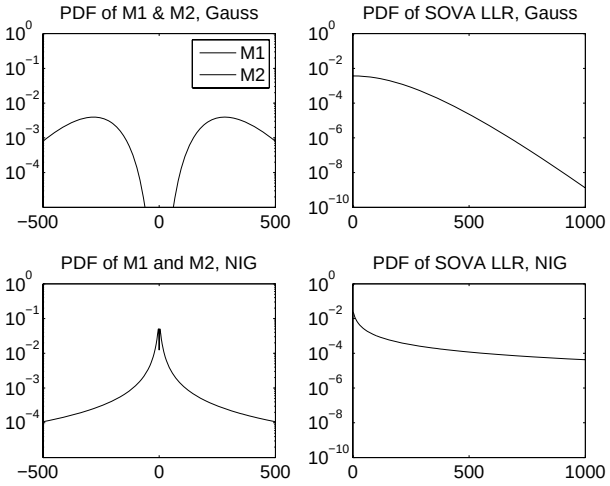

Fig. 18. PDF's of the SOVA accumulated cost function (left panels) and the decoder LLR estimates (right panels) in the case of Gaussian (upper panels) and NIG (lower panels) channel noise

For $0 < x < 1$ we approximate by

$$f_1(x) \;=\; l_N(1)x \tag{23}$$

This is a linear approximation using the fact that $l_N(0) = 0$. Using (12), the approximation $K_1(x) \approx \frac{1}{x}$ for small x and, according to the fit of Fig. 13, $\alpha, \delta << 1$ we get

$$\begin{aligned} q_p(1) &\approx \delta \\ q_m(1) &\approx 2 \\ l_N(1) &\approx \ln\{\frac{2}{\delta}\frac{K_1(\delta\alpha)}{K_1(2\alpha)}\} \approx \ln\{\frac{2}{\delta}\frac{1/(\delta\alpha)}{1/(2\alpha)}\} = 2\ln\frac{2}{\delta} \end{aligned} \tag{24}$$

For $x > 1$ we have

$$\begin{aligned} q_p &\approx x+1 \\ q_m &\approx x-1 \\ \ln\frac{x+1}{x-1} &\approx \frac{2}{x} \\ K_1(x) &\approx \sqrt{\frac{\pi}{2x}}e^{-x} \end{aligned} \tag{25}$$

Using (25) in the first part of (12) we get

$$\begin{aligned} l_N(x) &= \ln\{\frac{x+1}{x-1}\sqrt{\frac{\alpha(x+1)}{\alpha(x-1)}}e^{-\alpha(x-1)+\alpha(x+1)}\} \\ &= \frac{3}{2}\ln\frac{x+1}{x-1}+2\alpha \\ &= \frac{3}{x}+2\alpha \end{aligned} \tag{26}$$

We note that this approximation has the true value of 2α as x gets large. However, in order to get a continuous solution we adapt the value at $x=1$ and take the approximation to be

$$f_1(x) = \gamma x \tag{27}$$

$$f_2(x) = \frac{\gamma-2\alpha}{x}+2\alpha \tag{28}$$

defining $\gamma = 2\ln(2/\delta)$.

ACKNOWLEDGEMENT

The sea trials were made possible by extensive support from Kongsberg Maritime and FFI, both in terms of facilities and equipment. Questions regarding the NIG and MNIG distributions were helpfully answered by Preben Blæsild, Ole E. Barndorrf-Nielsen, and Tor-Arne Øigård. The constructive comments from associate editor Jim Preisig and the anonymous reviewers helped improve the quality of the manuscript.

REFERENCES

[1] C. Douillard, M. Jézéquel, C. Berrou, A. Picart, P. Didier, and A. Glavieux, "Iterative correction of intersymbol interference: Turbo-equalization," *Eur. Trans. Telecommunications*, vol. 6, pp. 507–511, September-October 1995.

[2] D. Raphaeli and A. Saguy, "Linear equalizers for turbo equalization: A new optimisation criterion for determining the equalizer taps," in *Proc. 2nd Int. Symp. on Turbo Codes & Related Topics*, (Brest, France), pp. 371–374, ENST Bretagne, Sept. 2000.

[3] A. Glavieux, C. Laot, and J. Labat, "Turbo equalization over a frequency selective channel," in *Proc. Int. Symp. on Turbo Codes & Related Topics*, (Brest, France), pp. 96–102, ENST Bretagne, Sept. 1997.

[4] M. Tüchler, R. Koetter, and A. C. Singer, "Turbo equalization: Principles and new results," *IEEE Trans. Communications*, vol. 50, pp. 754–767, May 2002.

[5] R. Otnes and M. Tüchler, "Iterative channel estimation for turbo equalization of time-varying frequency-selective channels," *IEEE Trans. Wireless Communications*, vol. 3, pp. 1918–1923, Nov. 2004.

[6] R. Galvin, R. F. W. Coates, L. S. Wang, and R. Stoner, "Measured channel sounding characteristics and their relationship with the performance of a parametric communication system," in *Proc. OCEANS '96*, vol. 2, (Fort Lauderdale, FL, USA), pp. 826–831, MTS/IEEE, Sept. 1996.

[7] V. Capellano, "Performance improvements of a 50 km acoustic transmission through adaptive equalization and spatial diversity," in *Proc. Oceans '97*, vol. 1, (Halifax, NS, Canada), pp. 569–573, MTS/IEEE, Oct. 1997.

[8] F. A. Blackmon and W. Canto, "Performance comparison of several contemporary equalizer structures applied to selected field test data," in *Proc. OCEANS 2000*, vol. 2, (Providence, RI, USA), pp. 809–816, MTS/IEEE, Sept. 2000.

[9] J. C. Preisig, "Performance analysis of adaptive equalization for coherent acoustic communications in the time-varying ocean environment," *J. Acoust. Soc. Am.*, vol. 118, pp. 263–278, July 2005.

[10] T. C. Yang, "Correlation-based decision-feedback equalizer for underwater acoustic communications," *IEEE J. Oceanic Engineering*, vol. 30, pp. 865–880, Oct. 2005.

[11] D. B. Kilfoyle, J. C. Preisig, and A. B. Baggeroer, "Spatial modulation experiments in the underwater acoustic channel," *IEEE J. Oceanic Engineering*, vol. 30, pp. 406–415, Apr. 2005.

[12] G. F. Edelmann, H. C. Song, S. Kim, W. S. Hodgkiss, W. A. Kupermann, and T. Akal, "Underwater acoustic communications using time reversal," *IEEE J. Oceanic Engineering*, vol. 30, pp. 852–864, Oct. 2005.

[13] E. M. Sozer, J. G. Proakis, and F. Blackmon, "Iterative equalization and decoding techniques for shallow water acoustic channels," in *OCEANS 2001*, vol. 4, (Honolulu. HI, USA), pp. 2201–2208, IEEE, Nov. 2001.

[14] F. Blackmon, E. Sozer, M. Murandian, J. Proakis, and M. Salehi, "Performance comparison of iterative/integral equalizer/decoder structures for underwater acoustic channels," in *Proc. MTS/IEEE Conf. OCEANS 2001*, vol. 4, (Honolulu, HI, USA), pp. 2191–2200, IEEE, Nov. 2001.

[15] D. B. Kilfoyle and A. B. Baggeroer, "The state of the art in underwater acoustic telemetry," *IEEE J. Oceanic Engineering*, vol. 25, pp. 4–27, Jan. 2000.

[16] R. Otnes, E. Slette, and E. Holmbakken, "Ideas for new serial-tone HF waveforms, optimized for turbo equalization," in *Proc. 7th Nordic Shortwave Conf., HF 04*, (Fårö, Sweden), pp. 6.4.1–6.4.10, Nordic Radio Society, Aug. 2004.

[17] R. Otnes and M. Tüchler, "Improved receivers for digital High Frequency waveforms using turbo equalization," in *Proc. MILCOM 2002*, vol. 1, (Anaheim, CA, USA), pp. 99–104, IEEE, Oct. 2002.

[18] R. Otnes, *Improved Receivers for Digital High Frequency Communications: Iterative Channel Estimation, Equalization, and Decoding (Adaptive Turbo Equalization)*. PhD thesis, Norwegian University of Science and Technology, Trondheim, Norway, Dec. 2002.

[19] R. Otnes, "Fractionally spaced linear MMSE turbo equalization," in *Proc. European Signal Processing Conference, EUSIPCO 2004*, (Vienna, Austria), pp. 465–468, EURASIP, Sept. 2004.

[20] M. Tüchler, A. C. Singer, and R. Koetter, "Minimum mean squared error equalization using *a priori* information," *IEEE Trans. Signal Processing*, vol. 50, pp. 673–683, Mar. 2002.

[21] R. Otnes and M. Tüchler, "Low-complexity turbo equalization for time-varying channels," in *Proc. 55th IEEE VTS Vehicular Technology Conf., VTC 2002 Spring*, vol. 1, (Birmingham, AL, USA), pp. 140–144, IEEE, May 2002.

[22] M. Tuchler *et al.*, "Graphical models for coded data transmission over inter-symbol interference channels," *European Transactions on Telecommunications*, pp. 307–321, 2004.

[23] X. Huang and N. Phamdo, "Turbo decoders which adapt to noise distribution mismatch," *IEEE Communications Letters*, vol. 2, pp. 321–323, Dec. 1998.

Dette er en postprint-versjon / This is a postprint version.
DOI til publisert versjon / DOI to published version: 10.1109/JOE.2008.925893

[24] L. Wei, Z. Li, M. R. James, and I. R. Petersen, "A minimax robust decoding algorithm," *IEEE Trans. Information Theory*, vol. 46, pp. 1158–1167, May 2000.

[25] A. Worm, P. Hoeher, and N. Wehn, "Turbo-decoding without SNR estimation," *IEEE Communications Letters*, vol. 4, pp. 193–195, June 2000.

[26] T. A. Summers and S. G. Wilson, "SNR mismatch and online estimation in turbo decoding," *IEEE Trans. Communications*, vol. 46, pp. 421–423, Apr. 1998.

[27] M. A. Khalighi, "Effect of mismatched SNR on the performance of log-MAP turbo detector," *IEEE Trans. Vehicular Technology*, vol. 52, pp. 1386–1397, Sept. 2003.

[28] Y. Huang and J. A. Ritcey, "EXIT chart analysis of BICM-ID over AWGN channel with SNR mismatch," *IEEE Communications Letters*, vol. 8, pp. 532–534, Aug. 2004.

[29] O. Barndorff-Nielsen, "Normal inverse Gaussian processes and stochastic volatility modelling," *Scand. J.Stat.*, pp. 1–13, May 1997.

[30] A. Hanssen and T. Oigard, "The normal inverse Gaussian distribution as a flexible model for heavy-tailed processes," in *IEEE-EURASIP Workshop on Nonlinear Signal and Image Processing*, p. 5 pages, June 2001.

[31] T. Oigard *et al.*, "EM-estimation and modeling of heavy-tailed processes with the multivariate normal inverse gaussian distribution," *Signal Processing, Elsevier*, pp. 1655–1673, 2005.

[32] A. Hanssen and T. Oigard, "The normal inverse Gaussian distribution: a versatile model for heavy-tailed stochastic processes," in *ICASSP '01*, pp. 3985 – 3988, May 2001.

[33] P. Blaesild, Feb. 2007. Personal correspondence.

[34] R. Otnes, "On soft-output demapping in filter-based soft-In/Soft-out equalizers," in *Proc. 3rd Int. Symp. on Turbo Codes and Related Topics*, (Brest, France), pp. 471–474, ENST Bretagne, Sept. 2003.

[35] A. Papoulis, *Probability, Random Variables and Stochastic Processes*. McGraw-Hill Inc., 1991.

[36] S. ten Brink, "Convergence behavior of iteratively decoded parallel concatenated codes," *IEEE Trans., Communications*, pp. 1727–1737, Oct 2001.

[37] J. Hagenauer and P. Hoeher, "A Viterbi algorithm with soft-decision outputs and its applications," in *Proc. IEEE Global Telecommunications Conf., GLOBECOM '89*, vol. 3, (Dallas, TX, USA), pp. 1680–1686, IEEE, Nov. 1989.

[38] L. R. Bahl, J. Cocke, F. Jelinek, and J. Raviv, "Optimal decoding of linear codes for minimizing symbol error rate," *IEEE Trans. Information Theory*, vol. IT-20, pp. 284–287, Mar. 1974.

[39] J. Proakis, *Digital Communications*. McGraw-Hill Inc., 2001.

[40] A. Salberg *et al.*, "The normal inverse Gaussian distribution as a model for MUI," in *ASILOMAR '01*, pp. 1484 – 1488, Nov 2001.